allow some study of the vehicle voltage versus current characteristics.

A search for optical auroras produced by the beam pulses was conducted with image-orthicon and image-intensifier cameras, Super-Schmidt meteor cameras, visual observers, photometers, and ballistic cameras located on the ground near Wallops Island and near Washington, D.C. These stations were provided with plots of look angles versus flight time for several possible rocket trajectories; the real trajectory was to be determined from radar data following burnout of the vehicle.

A search for electromagnetic radiation from the electron beam was conducted using two ground-based VLF stations, covering together the frequency range 500 hz to 12 khz, and narrow bands at 500 khz, 1.75 Mhz, and 2.9 Mhz. No positive results have been obtained to date from this search for electromagnetic radiation from the beam, indicating that lttle energy was emitted as waves.

The Aerobee 350 rocket carrying the accelerator experiment was launched from Wallops Island at 09:45 G.M.T. 26 January 1969. After burnout, the spinning of the rocket was stopped, and the rocket was reoriented with the electron guns pointing downward along $\overline{B}$. The nose cone was jettisoned and the electron collector screen deployed. Then the sealed electron guns were opened and electron beam pulsing began at approximately 235 km, continued through apogee at about 268 km, and was terminated by program at about 105 km. The maximum distance traversed by the beam was approximately 170 km. Reception was good, and all systems worked as intended.

The trajectory actually flown by the rocket was outside the anticipated path. As a result, no precalculated look angles were available, and the auroras were farther from the magnetic zenith of the prime optical observing station than had been intended. Nevertheless, auroras corresponding to the first four full-power pulses (490 ma at 8.7 kv for 1 second) were observed by two orthicon cameras. The auroras observed were long slender rays with a length (along $\overline{B}$) of 30 to 40 km and a width of 250 ± 50 m (Fig. 1). The pulse location, size, shape, and intensity are all roughly as expected. However, the spot width seems somewhat wider than calculated by Coulomb scattering stopping the beam. The intensity of auroral rays is close enough to the expected intensity that we are sure a substantial fraction of the electron beam power penetrated to about the 100 km level in the atmosphere. The experiment shows that beam propagation and stability problems were not too serious, and that producing auroras with electron beams is apparently feasible.

WILMOT N. HESS
Science and Applications Directorate, NASA Manned Spacecraft Center, Houston, Texas 77058

Note

1. This experiment was performed through the joint efforts of many people from several organizations. I acknowledge the cooperation and support of the following groups: NASA Goddard Space Flight Center; NASA Wallops Station; Ion Physics Corporation; Geophysical Institute, University of Alaska; Smithsonian Astrophysical Observatory; Radioscience Laboratory, Stanford University; Stanford Research Institute; U.S. Naval Research Laboratory; U.S. National Security Agency; School of Physics and Astronomy, University of Minnesota; Lockheed Palo Alto Research Laboratories; The Johns Hopkins University.

21 March 1969; revised 14 May 1969

Waterfall-Generated Earth Vibrations

Abstract. *Waterfalls generate periodic earth vibrations whose frequencies are inversely proportional to the height of the waterfall. Action of turbulent eddies is a probable explanation.*

Typically, a waterfall produces continuous earth vibration with one frequency predominating; this frequency is inversely proportional to the height of the waterfall. Frequency data for nine waterfalls in Iceland, Alaska, and continental United States, ranging in height from 5 to 93 m, were obtained with an HS-10 geophone, whose position, whether at the brink or the base of the fall, was immaterial (Fig. 1).

Waterfalls in which the flow is thoroughly broken up by ramps and ledges, such as a "horsetail" fall, have high background noise with no characteristic predominant frequency. While wide waterfalls—such as the Canadian and American Niagaras, also have high background noise—their predominate frequencies are discernible. Generally the data are not as consistent for low waterfalls as they are for high ones. A multiple-level fall, such as Gullfoss, a wide two-stage Icelandic waterfall, has as many characteristic frequencies as it has levels. Fourier analysis of the vibration frequencies of Gullfoss shows the two frequencies of 6 and 40 hz, which correspond, respectively, to drops of 7.5 and 27 m (Fig. 2).

While vibration set up in the earth must result from the water impinging

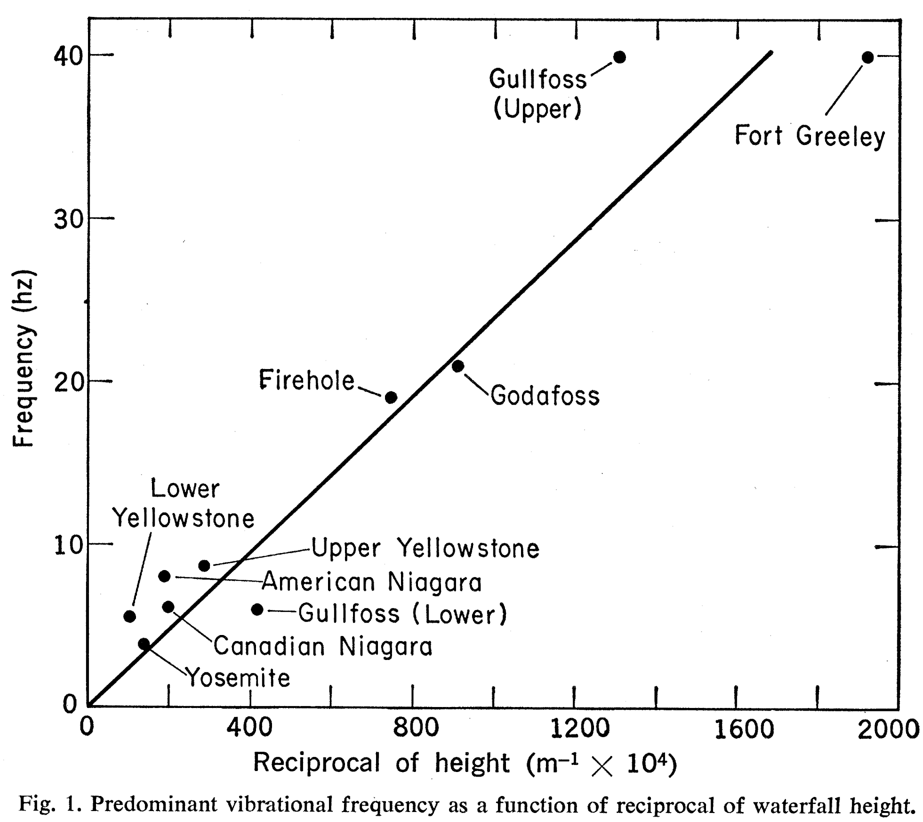

Fig. 1. Predominant vibrational frequency as a function of reciprocal of waterfall height.

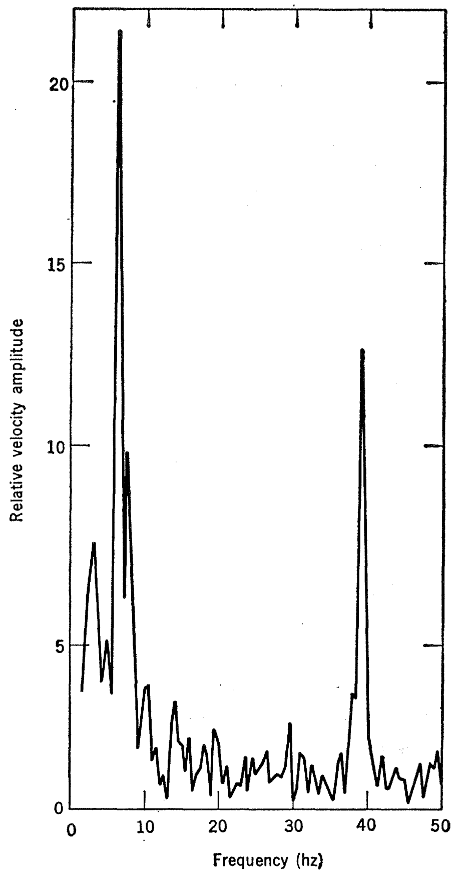

Fig. 2. Frequency spectrum of vibrations excited by Gullfoss.

against the base of the fall, details of the transfer of momentum are obscure. It is noteworthy that the slope of the solid line in Fig. 1 is 250 m/sec, about one-fourth the velocity of sound in water, suggesting that the entire water column may be resonating in the quarter wavelength mode. The impedance match at the base of the fall is good whereas that of the top is poor; this would place the node at the brink of the fall.

Water breaks up into discrete turbulent eddies as it falls, with the length of each eddy increasing with distance of fall. Such separation, which would give intermittent impacts and lower frequency with greater height, is clearly evident in most regular waterfalls. A small individual turbulent eddy usually does not maintain its identity the full length of fall. It grows in length and then melds with others to form larger and longer eddies, each of which strikes the base of the fall, producing strong earth motion.

JOHN S. RINEHART
Environmental Science Services Administration, Research Laboratories, Boulder, Colorado 80302

28 February 1969

Lunar Surface Material: Spacecraft Measurements of Density and Strength

Abstract. *The relation of the density of the lunar surface layer to depth is probably best determined from spacecraft measurements of the bearing capacity as a function of depth. A comparison of these values with laboratory measurements of the bearing capacity of low-cohesion particulate materials as a function of the percentage of solid indicates that the bulk density at the lunar surface is about 1.1 grams per cubic centimeter and that it increases nearly linearly to about 1.6 grams per cubic centimeter at a depth of 5 centimeters.*

Despite the successful landing of seven unmanned spacecraft on the moon, controversy continues about the density of lunar surface material. I present here further analysis of the available data.

With the Surveyor 7 soil mechanics surface sampler (*1*) the density of one surface rock was directly measured as 2.8 ± 0.4 g/cm^3. From the elemental chemical analyses made on the moon (*2*), model oxide compositions were derived that correspond to rock densities of 3.2 g/cm^3 in the maria sites of Surveyors 5 and 6, and 3.0 g/cm^3 at the Surveyor 7 site on the rim of Tycho (*3*). These values, however, pertain to the density of a fragment and of solid rock, rather than to the bulk density of the particulate layer that mantles the lunar surface.

A gamma-scattering densitometer on Luna 13 provided a direct indication of the bulk density. Unfortunately, the curve of density plotted against counting rate was double-valued, and the data fit a bulk density of about 0.8 g/cm^3 or greater than 2.1 g/cm^3 (*4, 5*). These values pertain to effective depths of 5 to 10 cm (*6*).

For particulate material of low cohesion, the static bearing capacity is a rather sensitive function of the percentage of solid and hence of the bulk density. Data on the static bearing capacity at various depths in the lunar surface layer are available from determinations of the loads imposed by a number of objects which made imprints on the surface and the corresponding bearing areas. The objects include a small rolling stone near Surveyor 5 (*7*), the head of the alpha-scattering instrument on Surveyor 7 (*8*), landing blocks on Surveyors 6 and 7 (*8, 9*), surface samplers used in bearing tests on Surveyors 3 and 7 (*1, 10*), a footpad on Surveyor 1 (*8, 9*), and a boulder that had rolled down the side of the crater Sabine D, as observed from Lunar Orbiter 2 (*11*). The imprint depth, bearing capacity, and bearing width for each object are shown in Table 1. The consistency of the Surveyor data is illustrated by a plot of bearing capacity against depth (Fig. 1); the data for width-to-depth ratios of 5 to 10 fall on a straight line through the origin, with a slope of about 1 newton/cm^3. Data for width-to-depth ratios of 0.8 to 1 fall at slightly lower bearing capacities, as would be expected from ordinary soil mechanics relations. The value for the Lunar Orbiter boulder indicates some decrease in the slope of the curve of bearing capacity versus depth at greater depths, as would be expected.

Laboratory tests of low-cohesion granular materials 7 to 70 percent solid indicate that a plot of bearing capacity p against percentage of solid s (*12*) can be fitted, within a scatter of 10 percent in s, by the relation

$$s = 20 \log p/p_0 \qquad (1)$$

where $p_0 = 0.016$ newton/cm^2. These tests used probes 0.6 to 2.8 cm in diameter under terrestrial gravity; cohesion of the materials tested was < 0.2 newton/cm^2. In the terrestrial tests for loosely packed material, with $s \leq 50$ percent, the bearing stress varied directly as the depth for fixed width; the plotted p was taken at a width-to-depth ratio of 1 (*12, 13*). Analysis for loosely packed material indicated that p should be independent of the gravitational acceleration (*13*) and should be only slightly dependent on bearing width (*14*). For densely packed material ($s > 50$ percent), the bearing capacity was reached at a small depth (high width-to-depth ratio), and the bearing stress increased very little with further increase in depth (*13*). For such material, analysis indicated that most of the bearing capacity would be provided by cohesion for bearing widths D (in centimeters) up to

$$D = 4 \times 10^4 \, c/g \qquad (2)$$

where c is the cohesion (in newtons per square centimeter) and g is the gravitational acceleration (in centimeters per second per second) (*13*).